Sensing and Bio-Sensing Research 4 (2015) 78–89

Contents lists available at ScienceDirect

Sensing and Bio-Sensing Research

journal homepage: www.elsevier.com/locate/sbsr

Sensing linear viscoelastic constitutive parameters with a Timoshenko beam on a multi-layer foundation: Modeling and simulation

Javad Fattahi, Davide Spinello *

Department of Mechanical Engineering, University of Ottawa, Ottawa, Ontario K1N 6N5, Canada

ARTICLE INFO

Keywords:
Viscoelastic response
Sensor model
Distributed parameter system
Inverse problem

ABSTRACT

We present a sensor model comprised of a Timoshenko beam coupled with a linear viscoelastic substrate via a distributed system of compliant elements. The system of governing equations includes the evolution of the kinematic descriptors of the Timoshenko beam and of the interface between the coupling elements and the viscoelastic substrate. This model is used to pose an inverse problem aimed at estimating the constitutive parameters of the substrate from deformation measurements of the beam. The sensing model is demonstrated by comparing its prediction with published experimentally obtained constitutive parameters identifying standard linear viscoelastic material models, showing good agreement between model estimations and experimental results.

1. Introduction

We propose a model for a continuous deformable system that can be used as a sensor to estimate constitutive parameters of a substrate to which it is coupled. The sensor is comprised of a planar Timoshenko beam, and of a distributed system of compliant elements that exert the coupling with the substrate. The system is a sensor in the sense that kinematic quantities (that is, deflections and rotations along the axis of the beam) are acquired through measurements; the model of the system allows then to define a cost function that encodes least square residuals between measurements and model displacements, including constitutive parameters that can be estimated by minimizing the cost function. This leads naturally to an inverse problem formulation, in which the action or external forces (from the substrate) that determine a given kinematics (measured) has to be found, as it is ultimately related to the material response of the substrate and therefore to the estimation of constitutive parameters. One important application of this work is the estimation of material parameters for soft biological tissues, which is demonstrated by comparison of the predictions of the proposed model with published results.

Inverse problems is a branch of research whose scope can be broadly defined as the inversion of models or data to find unknown properties of a related system [1]. This framework applies to a wide range of engineering and science applications, such as the estimation of spatial and temporal-dependent external forces in dynamical systems [2], the estimation of transient heat transfer rates in thermal systems [3], the estimation of forced convection in parallel plate channels [4,5], and the estimation of surface heat flux in thermal problems [6]. An important class of applications that include the work presented in this paper is the one concerning the estimation of material parameters in constitutive relations of elastoplastic and viscoelastic materials, often modeled in the framework of continuum mechanics. An algorithm to solve inverse problems in linear elasticity is presented in [7], and an in inverse problem to estimate constitutive parameters in elastoplastic solids in presented in [8]. Full-field measurements techniques are presented in [9,10] to estimate elastic parameters in solids, and a model-based approach is used in [11] to estimate viscoelastic response constitutive parameters. A numerical technique based on finite elements method is presented in [12] to estimate material parameters from displacement and force measurements. Applications to the estimation of material parameters in geotechnical applications, that typically involve the response of soils or similar substrates, are presented in [13]. This work advances in the framework of inverse problems, by proposing the model of a sensing system that allows to estimate the viscoelastic response parameters of a layer coupled with a deformable body through a distributed system of compliant elements. The system's model describes the evolution of the deformable body and of the interface of the substrate, and material parameters are estimated by finding the minimizers of a least square metric that encodes the distance between measured kinematic quantities and corresponding ones from the model.

Inverse problems for hyper redundant mechanisms with different geometric and dynamic conditions include: dynamic modeling of multi-link flexible robotic manipulators [14], calibration of

* Corresponding author.

http://dx.doi.org/10.1016/j.sbsr.2015.04.003
2214-1804/

model parameters of flexible manipulator [15], model reduction of rigid-flexible manipulators [16], the approximation of state space equations of flexible link manipulators [17], and modeling and trajectory planning of mobile manipulators with flexible links [18,19]. For elongated hyper-redundant systems, models of one dimensional continua with local Euclidean structure (beam models) are often naturally adopted, due to their suitability in describing the features associated with the slenderness. Many studies have been dedicated to inverse problems applied to structural health monitoring, crack identification, or to the estimation of material properties of soils. Among all, micro-channel heater/evaporators for thermal phase-change actuators have been presented in [20]; a PM-PCF vibration sensor for structural health monitoring of composite is presented in [21]; the inverse mode problem with application to structural health monitoring is addressed in [22] by a discretization approach, in [23] by a quadratic inverse eigenvalue approach, and in [24] by a variational approach. Additional works proposing methods to tackle nonlinear inverse problems in vibrations are [25–27]. An inverse vibrations problem to monitor and inspect the structural integrity of multi-story building is formulated in [28], whereas an experimental approach based on vibration measurements is presented in [29] for crack identification in structural members. A crack detection technique based on a dynamic stiffness inverse vibration formulation is presented in [30,31]; within the same framework, a nonlinear inverse problem approach to estimate the external forces in displacement-dependent parameters models is presented in [32,33].

In inverse problem solutions, different optimization techniques are used to estimate time dependent parameters, often related to root searching iterative methods belonging to the family of steepest descent and scaled steepest descent methods. Textbook [34] present general methods of solution of inverse problems for vibrating systems. Inverse vibration problems with parameter uncertainty are studied in [35]; a symmetric inverse vibration problem is presented in [36], and the application of different optimization methods to the solution of inverse problems for linear and nonlinear vibrating and static systems can be found in [37,38]. Within the same framework, an anharmonic vibration inverse problem with reconstruction of Hamiltonian terms is studied in [39]; shape determination problems of structures by an inverse variational principle is reported in [40]; conditions for the uniqueness of solution of a specific inverse vibration problem is presented in [41].

Additionally, the estimation of mechanical properties is crucial in the investigation of stability, development, and remodeling of biological tissues. The constitutive response of biomaterials can be correlated to the physical structure of living tissues and with eventual abnormalities, resulting into diagnosing techniques [42,43]. The links between biomechanics and human diseases have been the subject of considerable scientific research efforts [44–47]. Recent developments of the study of biological systems has reached a point where it can benefit considerably from contributions from continuum mechanics, which have provided a framework to analyze and predict the behavior of biomechanical mechanisms without specifically modeling the properties at the cellular and molecular levels [48–50].

For coupled system presented in this work, measured quantities are strains and/or displacements along the body of the beam, where the bending is the input in the corresponding inverse problem. More specifically, by modeling the material response of the substrate with a simple linear viscoelastic model, we pose an estimation problem in which, by measuring deformations and/or stresses on the beam, we can infer the material properties of the substrate. In this case, the overall coupled system is modeled as a beam on a multi-layer foundation, where different layers have different material responses. A least square distance between measurements and displacements from the model allow to estimate encoded material parameters through a standard minimization procedure. This class of numerical optimization tools has been used in [51,52] to estimate time dependent material parameters, and in [53–55] to solve inverse problems in linear and non-linear vibrating systems. Predictions of this sensor model are in good agreement with published results, suggesting that the system can be used in a versatile way as an autonomous agent operating in a generic environment, and simultaneously as a sensor that could inform the action of the system itself [56], or that could be used to monitor the environment. The modeling work done in this study opens can be implemented in engineering systems applied to environmental monitoring and health applications, in which we envision the system to be used to estimate material properties of living tissues, that can be correlated to the diagnosis of classes of diseases.

The rest of paper is organized as follows. In Section 2 we present the model of a linear Timoshenko beam coupled with a viscoelastic foundation by a continuous distribution of compliant elements. The viscoelastic foundation represents linear viscoelastic materials for which we want to estimate constitutive parameters. This setting allows to formulate the problem as the one of a beam on a multi-layer foundation. A reduced order model for the beam on viscoelastic foundation is then derived, to allow to solve the coupled system of governing partial differential equations. In Section 3 we formulate the inverse problem to estimate constitutive parameters of the substrate. Results and discussions are presented in Section 4.

2. Mechanical model of the coupled system

In this section we present the mechanical model of a deformable body coupled with a viscoelastic substrate through a distributed system of deformable elements. The deformable body along with the distributed system of coupling elements is inspired by a class of organisms that move on unstructured substrates by adapting the shape of their bodies to non-zero curvatures of the substrates (shape morphing) and by forward locomoting through a traveling wave-like motion transmitted by the legs in contact with the substrate. These features have been used in [57,56] to model and simulate shape morphing and forward locomotion. Here, these ideas are extended to exploit the system's features as a sensor, in which case the shape morphing parameters are observable (measured) and suitable characteristics of the substrate are reconstructed based on the model presented below. Specifically, we consider an elastic elongated body on a generalized foundation, where the two layers of the foundation are provided by the coupling system and by the substrate, see schematics in Fig. 1. The governing equations of the system include the evolution of the Timoshenko beam and of the interface between the substrate and the coupling elements.

2.1. Sensor's body model

We are interested in describing the kinematics of a deformable body that can be considered as the limit of a sequence of rigid elements connected through soft elements acting as spherical joints. This reproduces the salient characteristics of the bodies of millipedes [58–60] that specifically characterizes their peculiar shape morphing coupled with forward locomotion. In order to retain the independent relative rotational motion between two contiguous elements, it is natural to adapt a Timoshenko beam model that is a one dimensional continuum (axis) with a local Euclidean structure describing the state of cross section [56]. We consider the variation of the curvature of the substrate to be small, and the mechanism to be locally parallel to the substrate, which implies

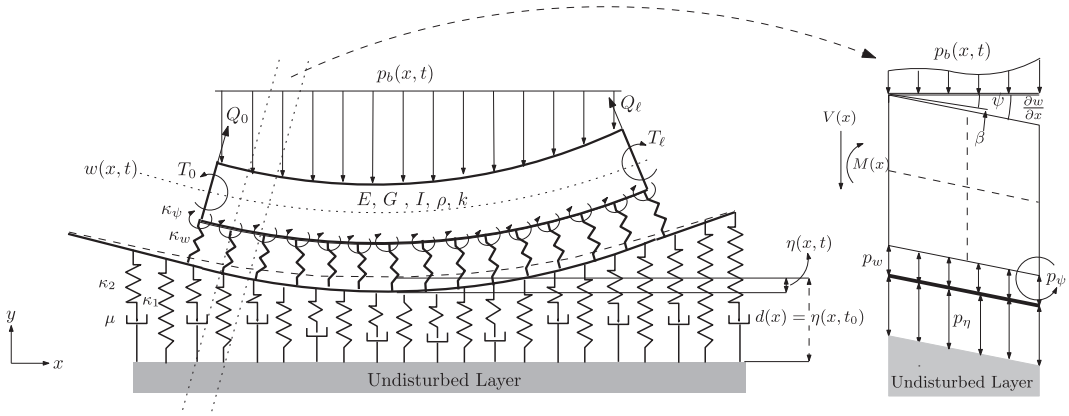

Fig. 1. Schematics of a planar Timoshenko beam coupled with a viscoelastic foundation, and detail of the free body diagram of a portion of the beam.

that deformations are small [61]. Let $\{x, y, z\}$ be a fixed rectangular Cartesian frame with $x \in [0, L]$ spanning the initially rectilinear axis of the beam, and $\{y, z\}$ spanning the beam's cross section. By referring to Fig. 1, let u be the axial displacement, ψ be the rotation angle of the cross section, and w be the transverse displacement. The linear planar Timoshenko beam is then described by the following set of evolution equations

$$\varrho A\frac{\partial^2 u}{\partial t^2} + c_u\frac{\partial u}{\partial t} = \frac{\partial}{\partial x}\left(EA\frac{\partial u}{\partial x}\right) + p_u \tag{1a}$$

$$\varrho A\frac{\partial^2 w}{\partial t^2} + c_w\frac{\partial w}{\partial t} = \frac{\partial}{\partial x}\left(kAG\left(\frac{\partial w}{\partial x} - \psi\right)\right) + p_w \tag{1b}$$

$$\varrho I\frac{\partial^2 \psi}{\partial t^2} + c_\psi\frac{\partial \psi}{\partial t} = \frac{\partial}{\partial x}\left(EI\frac{\partial \psi}{\partial x}\right) + kAG\left(\frac{\partial w}{\partial x} - \psi\right) + p_\psi \tag{1c}$$

where ϱ is the volume mass density, A the area of the cross section, I the moment of inertia, E and G respectively Young's and shear elastic moduli, k is the shear modulus (nondimensional parameter that depends on the geometry), and p_u, p_w, and p_ψ are distributed loads (per unit length) in the axial and transverse directions and a distributed couple perpendicular to the plane of motion. Terms proportional to the first time derivatives through coefficients c_u, c_w, and c_ψ model the structural damping as equivalent viscous damping [62]. Structural damping accounts for hysteresis phenomena in elastic materials undergoing cyclic loading [62,63], and therefore it depends on the frequency of excitation. In equivalent viscous damping models the dependency on the frequency of excitation $\bar{\omega}$ is included through the proportional coefficients by the inverse law $c_u = \bar{c}_u/(\pi\bar{\omega})$ (similarly for c_w and c_ϕ) [63], where $\bar{c}_u$ is a constant independent of $\bar{\omega}$.

We consider the following force (von Neumann) boundary conditions

$$\text{At } x = 0: \quad kAG\left(\frac{\partial w}{\partial x} - \psi\right) + Q_0 = 0, \quad EI\frac{\partial \psi}{\partial x} + T_0 = 0 \tag{2a}$$

$$\text{At } x = \ell: \quad -kAG\left(\frac{\partial w}{\partial x} - \psi\right) + Q_\ell = 0, \quad -EI\frac{\partial \psi}{\partial x} + T_\ell = 0 \tag{2b}$$

where Q_0, Q_ℓ and T_0, T_ℓ are respectively shear forces and bending moments applied at the boundaries $x = 0$ and $x = \ell$, see Fig. 1.

2.2. Substrate model

Fig. 1 shows a Timoshenko beam supported by a system of distributed compliant elements connected with a substrate with viscoelastic response. For linear viscoelastic materials, the relation between stress and strain is a function of strain and strain rate. With reference to Fig. 2, typical linear viscoelastic responses have lumped representations described by Kelvin–Voigt, Maxwell, and standard linear models. The standard linear model is used to describe the linear viscoelastic response of a number of soft and biological materials, among others. The constitutive relation for the standard linear model is [64]

$$\kappa_1\sigma + \mu\dot{\sigma} = \kappa_1\kappa_2\varepsilon + \mu(\kappa_1 + \kappa_2)\dot{\varepsilon} \tag{3}$$

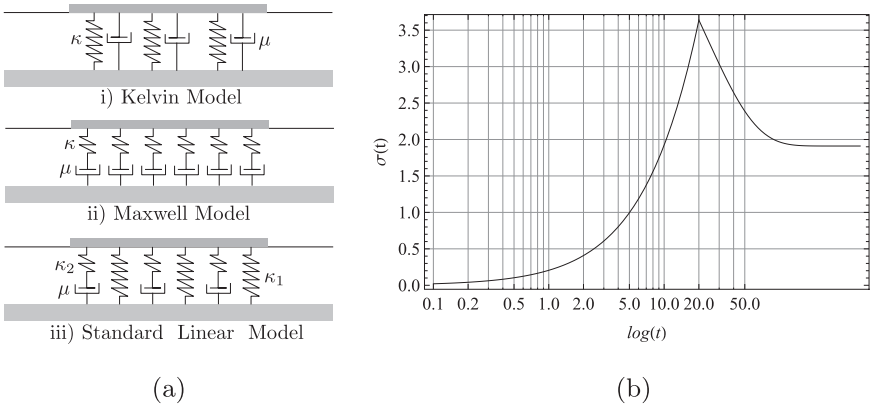

Fig. 2. (a) Three linear viscoelastic models and (b) stress-relaxation response of an standard linear viscoelastic model with κ_1=2 Nm^{-1}, κ_2 =1.5 Nm^{-1}, μ =20 Nsm^{-1}.

where σ is the normal stress, ε is the normal strain, a superimposed dot means material time differentiation, and κ_1, κ_2, and μ are stiffness and damping parameters of the elements represented in Fig. 2, having the physical dimensions of elastic and viscous moduli, respectively. Here we defined normal stress and normal strain by considering a continuous distribution of lumped elements. By referring to Fig. 1 we define the undeformed profile of the substrate to be $d(x)$, and the deformation of the same profile with respect to the undeformed configuration to be $\eta(x,t)$. The profile $d(x)$ can be interpreted as the thickness of a viscoelastic layer with respect to the depth of a layer that is not affected by the interaction with the beam, so that the normal strain ε in the viscoelastic model can be expressed as $\varepsilon = \eta/d$. Considering p_η as the normal force per unit width of the substrate exerted by the viscoelastic layer, we can rewrite the balance in (3) as

$$\kappa_1 p_\eta + \mu \dot{p}_\eta = \kappa_1 \kappa_2 \frac{\eta}{d} + \mu(\kappa_1 + \kappa_2)\frac{\dot{\eta}}{d} \tag{4}$$

2.3. Model of the coupled system

The sensing system modeled in this work is comprised of a deformable body coupled with a substrate through a distributed set of compliant elements. In order to describe the coupling between the different parts we adopt a multi-layer foundation model with a beam resting on it. Specifically, the foundation model is comprised of two layers respectively representing the coupling elements and the viscoelastic substrate. Following [65] we obtain an evolution equation for the interface between the two layers that is coupled with the evolution of the body described as a Timoshenko beam. The solution of the evolution of the interface describes the profile of the substrate to which the sensor is deployed. Different elastic and viscoelastic foundation models have been introduced to appropriately describe relevant scenarios [65]. The simplest is the Winkler model, in which the foundation is described as a system of independent springs reacting to the deflection of the body [66,67]. Two parameters extensions of the Winkler model have been proposed by Filonenko-Borodich [68] and Pasternak [69–71] respectively by considering membrane like interactions (with constant tension) and shear interactions among springs. Alternatively to this family of models that are based on interactions between mechanical elements, continuum medium based model have been proposed based on variational formulations that include assumed kinematics of the foundation elastic medium [66,72]. The Vlasov model [73] is based on the assumption that the in-plane displacement of the structure is identically zero, and the displacement on the transverse direction is controlled by the structure's deflection through a shape function that expresses the dependency on the depth of the elastic medium. A rigorous derivation of the shape function of the Vlasov model is presented in [72]. The generalized Vlasov-Jones model is presented in [74] to account for non-vanishing in-plane structural displacements, and adapted in [75] to describe the isotropic matrix material in syntactic foams particulate composites. All two parameter models are equivalent in the sense that they are described by the same constitutive relation, except for the computation of the parameters [76].

To describe the interaction between the coupling elements and the body we adopt a generalized foundation model [76], in which the coupling elements transfer a distributed force and a distributed couple constitutively related to the kinematics of the Timoshenko beam and to the interface deformation descriptor η. By introducing the external body forces p_b and external body couples p_c we specify the forces and couples in (1) by

$$p_w = p_b - \kappa_w(w-\eta), \quad p_\psi = p_c - \kappa_\psi\left(\psi - \frac{\partial \eta}{\partial x}\right) \tag{5}$$

where κ_w and κ_ψ (respectively with SI physical dimensions $\mathrm{Nm^{-2}}$ and $\mathrm{Nm^{-1}}$) are elastic constants associated to linear and rotational distributed springs. Therefore the coupling elements relate the profile η and its slope to the kinematics of the Timoshenko beam. In the sensing framework p_b and p_c can be considered as inputs to the system that allow to estimate constitutive parameters, as specified below. The reactions $-\kappa_w(w-\eta)$ and $\kappa_\psi(\psi - \partial\eta/\partial x)$ are measured with respect to the static reactions $-\kappa_w d$ and $\kappa_\psi \partial d/\partial x$, and therefore $d(x)$ can be considered as the initial undisturbed profile under static equilibrium conditions. Additionally, we assume $p_u = 0$ as we consider only the deflection of the body. To obtain the evolution of the interface we assume that only normal interactions are transmitted through it, that is the coupling elements and the substrate interact only through normal forces. More general multi-layer foundations consider shear interactions as well [77]. The balance of normal forces at the interface gives

$$-\kappa_w(w-\eta) + p_\eta = 0 \tag{6}$$

Substituting (6) into (4) we obtain the evolution equation for the interface that has initial undisturbed profile $d(x)$

$$\kappa_1\kappa_w(w-\eta) + \mu\kappa_w(\dot{w}-\dot{\eta}) - \kappa_1\kappa_2\frac{\eta}{d} - \mu(\kappa_1+\kappa_2)\frac{\dot{\eta}}{d} = 0 \tag{7}$$

2.4. Nondimensional Governing Equations

We introduce the nondimensional variables

$$\hat{x} = \frac{x}{\ell}, \quad \hat{t} = \frac{t}{\tau}, \quad \hat{w} = \frac{w}{\ell}, \quad \hat{p}_b = \frac{p_b}{\kappa_w \ell}, \quad \hat{p}_c = \frac{p_c}{\kappa_\psi \ell}, \quad \hat{\eta} = \frac{\eta}{\ell}, \quad \hat{d} = \frac{d}{\ell} \tag{8}$$

where ℓ is the total length of the undeformed body, and τ is the characteristic time that is given by

$$\tau^2 = \frac{\varrho \ell^2}{kG} \tag{9}$$

By substituting (5) into (1b), (1c) and (7), we rewrite the governing equations in nondimensional form as

$$\frac{\partial^2 w}{\partial t^2} + \frac{\alpha_w}{\omega^\star}\frac{\partial w}{\partial t} - \frac{\partial^2 w}{\partial x^2} + \frac{\partial \psi}{\partial x} + \alpha_3 w = p_b + \alpha_3 \eta \tag{10a}$$

$$\alpha_1\frac{\partial^2 \psi}{\partial t^2} + \frac{\alpha_\psi}{\omega^\star}\frac{\partial \psi}{\partial t} - \frac{\partial^2 \psi}{\partial x^2} + \alpha_4\psi - \alpha_1\alpha_2\left(\frac{\partial w}{\partial x} - \psi\right) = p_c + \alpha_4\frac{\partial \eta}{\partial x} \tag{10b}$$

$$\beta_1(w-\eta) + \beta_\mu(\dot{w}-\dot{\eta}) - \beta_1\beta_2\frac{\eta}{d} - \beta_\mu(\beta_1+\beta_2)\frac{\dot{\eta}}{d} = 0 \tag{10c}$$

Here we have dropped the hat to indicate nondimensional quantities, and we have introduced the nondimensional groups

$$\alpha_1 = \frac{kG}{E}, \quad \alpha_2 = \frac{A\ell^2}{I}, \quad \alpha_3 = \frac{\kappa_w \ell^2}{kAG}, \quad \alpha_4 = \frac{\kappa_\psi}{EI} \tag{11a}$$

$$\omega^\star = \bar{\omega}\tau, \quad \alpha_w = \frac{\bar{c}_w \ell^2}{\pi k A G}, \quad \alpha_\psi = \frac{\bar{c}_\psi \ell^2}{\pi E I} \tag{11b}$$

$$\beta_1 = \frac{\kappa_1}{\kappa\ell}, \quad \beta_2 = \frac{\kappa_2}{\kappa\ell}, \quad \beta_\mu = \frac{\mu}{\kappa\ell\tau}. \tag{11c}$$

Therefore $\alpha_1\alpha_2$ is a measure of the shear stiffness versus the bending stiffness, α_3 is a measure of the legs' linear stiffness versus the shear stiffness, α_4 measures the leg's bending stiffness with respect to the bending stiffness of the body, and α_w and α_ψ are structural damping factors.

The nondimensional version of boundary conditions (2) is

$$\text{At } x=0: \quad \frac{\partial w}{\partial x}-\psi+\widehat{Q}_0=0, \quad \frac{\partial \psi}{\partial x}+\widehat{T}_0=0 \tag{12a}$$

$$\text{At } x=\ell: \quad -\left(\frac{\partial w}{\partial x}-\psi\right)+\widehat{Q}_1=0, \quad -\frac{\partial \psi}{\partial x}+\widehat{T}_1=0 \tag{12b}$$

where nondimensional forces and torques $\widehat{Q}$ and $\widehat{T}$ are obtained from the corresponding dimensional ones respectively by dividing by kAG and by EI. Since no ambiguity arises, in the following we will drop the hat for nondimensional boundary forces and torques. By assuming that only the portion of the substrate in contact with the sensor experiences deformation, we adopt the following boundary conditions for the field η

$$\eta(x,t)=0 \text{ at } x=0 \text{ and } x=1. \tag{13}$$

2.5. Reduced Order Model

We obtain a reduced order model for the coupled system (10) through Galerkin projections of the fields w, ψ, and η on suitable bases. By separation of variables, the kinematic fields are expressed as

$$w(x,t)=\bar{\mathbf{w}}^{\mathsf{T}}(x)\mathbf{a}(t) \tag{14a}$$

$$\psi(x,t)=\bar{\boldsymbol{\psi}}^{\mathsf{T}}(x)\mathbf{b}(t) \tag{14b}$$

$$\eta(x,t)=\bar{\eta}(x)c(t) \tag{14c}$$

where $\bar{\mathbf{w}}=(\bar{w}_1\cdots\bar{w}_n)^{\mathsf{T}}, \bar{\boldsymbol{\psi}}=(\bar{\psi}_1\cdots\bar{\psi}_n)^{\mathsf{T}}$, and $\bar{\eta}$ are spatial basis functions. Basis functions $\bar{\mathbf{w}}$ and $\bar{\psi}$ are obtained by solving the vector eigenvalues problem associated with a planar Timoshenko beam with free end boundary conditions, see [56] and the Appendix for details. Mode shapes are normalized with respect to the maximum amplitude. Plots of the first three modes $\bar{\mathbf{w}}$, and $\bar{\psi}$ normalized with respect to the maximum value are given in Fig. 3. The interface η is considered as a small deformation with respect to the undeformed profile $d(x)$, and the basis function $\bar{\eta}$ is chosen to be a quadratic polynomial satisfying homogeneous boundary conditions

$$\bar{\eta}(x)=x(x-1) \tag{15}$$

Coefficients $\mathbf{a}=(a_1\cdots a_n)^{\mathsf{T}}, \mathbf{b}=(b_1\cdots b_n)^{\mathsf{T}}$ and $c(t)$ represent unknown time dependent amplitudes. By introducing the matrices (see Appendix B for more details)

$$\mathbf{M}_1=\int_0^1 \bar{\mathbf{w}}\bar{\mathbf{w}}^{\mathsf{T}}\mathrm{d}x, \quad \mathbf{M}_2=\int_0^1 \bar{\boldsymbol{\psi}}\bar{\boldsymbol{\psi}}^{\mathsf{T}}\mathrm{d}x, \quad M_3=\int_0^1 \bar{\eta}^2\mathrm{d}x \tag{16a}$$

$$\mathbf{K}_1=\int_0^1 \frac{\mathrm{d}\bar{\mathbf{w}}}{\mathrm{d}x}\frac{\mathrm{d}\bar{\mathbf{w}}^{\mathsf{T}}}{\mathrm{d}x}\mathrm{d}x, \quad \mathbf{K}_2=\int_0^1 \frac{\mathrm{d}\bar{\boldsymbol{\psi}}}{\mathrm{d}x}\frac{\mathrm{d}\bar{\boldsymbol{\psi}}^{\mathsf{T}}}{\mathrm{d}x}\mathrm{d}x, \quad K_3=\int_0^1 \frac{\bar{\eta}^2}{d}\mathrm{d}x \tag{16b}$$

$$\mathbf{K}_{w\psi}=\int_0^1 \frac{\mathrm{d}\bar{\mathbf{w}}}{\mathrm{d}x}\bar{\boldsymbol{\psi}}^{\mathsf{T}}\mathrm{d}x, \quad \mathbf{K}_{\eta w}=\int_0^1 \bar{\eta}\bar{\mathbf{w}}\mathrm{d}x, \quad \mathbf{K}_{\psi\eta}=\int_0^1 \bar{\boldsymbol{\psi}}^{\mathsf{T}}\frac{\mathrm{d}\bar{\eta}}{\mathrm{d}x}\mathrm{d}x \tag{16c}$$

we obtain the reduced order model in the form of the following coupled ordinary differential equations for the amplitudes $\mathbf{a}(t), \mathbf{b}(t)$ and $c(t)$

$$\mathbf{M}_1\ddot{\mathbf{a}}(t)+\frac{\alpha_w}{\omega^\star}\mathbf{M}_1\dot{\mathbf{a}}(t)+(\mathbf{K}_1+\alpha_3\mathbf{M}_1)\mathbf{a}(t)-\mathbf{K}_{w\psi}\mathbf{b}(t)-\alpha_3\mathbf{K}_{\eta w}^{\mathsf{T}}c(t)=\mathbf{F}_w(t) \tag{17a}$$

$$\alpha_1\mathbf{M}_2\ddot{\mathbf{b}}(t)+\frac{\alpha_\psi}{\omega^\star}\mathbf{M}_2\dot{\mathbf{b}}(t)+(\mathbf{K}_2+(\alpha_1\alpha_2+\alpha_4)\mathbf{M}_2)\mathbf{b}(t)-\alpha_1\alpha_2\mathbf{K}_{w\psi}^{\mathsf{T}}\mathbf{a}(t) - \alpha_4\mathbf{K}_{\psi\eta}c(t)=\mathbf{F}_\psi(t) \tag{17b}$$

$$\beta_\mu(M_3+(\beta_1+\beta_2)K_3)\dot{c}(t)+\beta_1(M_3+\beta_2K_3)c(t) - \mathbf{K}_{\eta w}\left(\beta_1\mathbf{a}(t)+\beta_\mu\dot{\mathbf{a}}(t)\right)=0 \tag{17c}$$

where forcing terms $\mathbf{F}_w$ and $\mathbf{F}_\psi$ are given by

$$\mathbf{F}_w=-(Q_0\bar{\mathbf{w}}(0)+Q_1\bar{\mathbf{w}}(1))+\int_0^1 p_b\bar{\mathbf{w}}\mathrm{d}x \tag{18a}$$

$$\mathbf{F}_\psi=-\left(T_0\bar{\boldsymbol{\psi}}(0)+T_1\bar{\boldsymbol{\psi}}(1)\right)+\int_0^1 p_c\bar{\boldsymbol{\psi}}\mathrm{d}x \tag{18b}$$

Forces and moments in (18) can be considered as inputs to the sensor system, with corresponding deformations and internal forces obtained by measurements.

3. Inverse Problem

In this section we present a procedure to use the model described in Section 2 to estimate the material properties of the viscoelastic layer, see Fig. 4. The model for the coupled system is given by the set of Eqs. (10), which describe the coupled evolution of the beam and of the interface between the substrate and the coupling elements. We formulate an inverse problem based on the model (10) to estimate the material parameters of the substrate given displacement and/or force measurements of the beam.

The general structure of the inverse problem is schematized in Fig. 5, where a least squares residuals cost function is build from measurements and the model, and material parameters are selected as minimizers of such cost function. As specified below, different cost functions can be defined based on the nature of measurements, for example by considering either a displacement sensor or a force sensor.

3.1. Displacement sensor

When using the system as a displacement sensor, a time series of displacements of the beam are taken at a set of observation points $x_1,\ldots,x_n$ along the axis of the beam. Such time series measurements can be typically collected by a system of strain gauges or other common strain sensors while the system responds to a suitable excitation. In a current implementation being developed at the University of Ottawa, the body of the sensor has been realized with silicon, and strains at observation points along the body will be measured by strain gauges. Because of the material of the

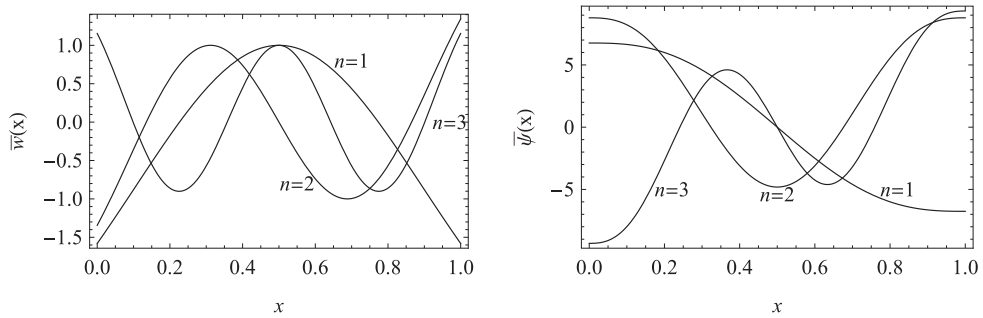

Fig. 3. First three bending and rotational modes, normalized with respect to the maximum value along the beam's span.

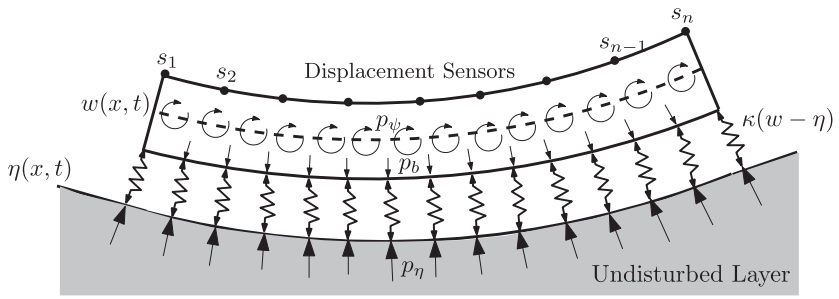

Fig. 4. Schematic for the sensor system with set of observation points $(s_1, s_2, \cdots, s_n)$ along the beam axis.

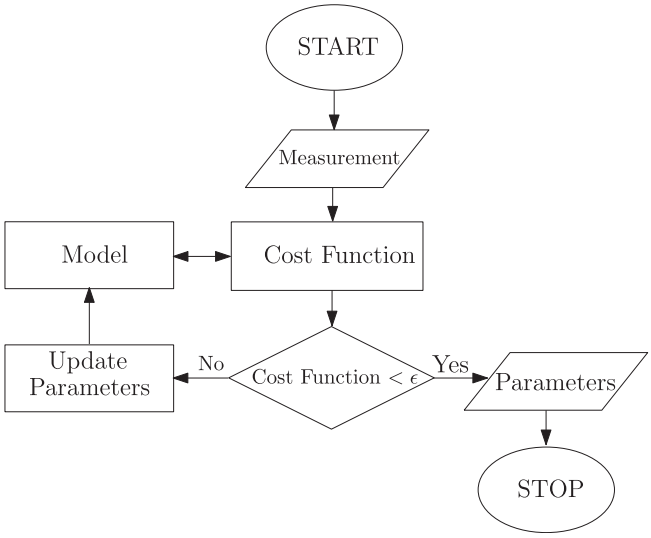

Fig. 5. General flowchart of inverse problem.

body and of its flexibility, specific attention needs to be put in selecting the appropriate adhesive to glue the strain gauges. An alternative, inexpensive solution is offered by flex sensor, that are considerably less expensive than strain gauges. However, they give qualitative measurements at best, and they can bias the deflection of the beam as they can be quite long and invasive. The choice of sensing devices mounted on the system ultimately determine important parameters such as bandwidth and resolution. Relatively inexpensive strain-gauges currently available can be very high resolution. Sensing inaccuracies are numerically investigated in the section dedicated to results, by considering measurements with different, relatively high noise. At time t, the spatial sets of displacements are denoted by the collections

$$\tilde{\mathbf{w}}(t) = (\tilde{w}_1(t), \ldots, \tilde{w}_n(t))^{\mathsf{T}} \tag{19a}$$

$$\tilde{\boldsymbol{\psi}}(t) = \left(\tilde{\psi}_1(t), \ldots, \tilde{\psi}_n(t)\right)^{\mathsf{T}} \tag{19b}$$

In order to estimate the material parameters corresponding to the model (10) we define the least square residuals cost function by

$$\mathscr{R}(\hat{\mathbf{g}}) = \frac{1}{2}\sum_{j=1}^{N}\Big(\big(\tilde{\mathbf{w}}(t_j) - \mathbf{w}(\hat{\mathbf{g}}, t_j)\big)^{\mathsf{T}} \big(\tilde{\mathbf{w}}(t_j) - \mathbf{w}(\hat{\mathbf{g}}, t_j)\big) + \big(\tilde{\boldsymbol{\psi}}(t_j) - \boldsymbol{\psi}(\hat{\mathbf{g}}, t_j)\big)^{\mathsf{T}} \big(\tilde{\boldsymbol{\psi}}(t_j) - \boldsymbol{\psi}(\hat{\mathbf{g}}, t_j)\big)\Big) \tag{20}$$

where $\hat{\mathbf{g}}$ is a set of estimated parameters, that in this case include the viscoelastic constitutive parameters of the substrate, that is $\hat{\mathbf{g}} = (\hat{\beta}_{f_1}, \hat{\beta}_{f_2}, \hat{\beta}_\mu)$;

$$\mathbf{w}(\hat{\mathbf{g}}, t) = (w(x_1, t), \ldots, w(x_n, t))^{\mathsf{T}}, \quad \boldsymbol{\psi}(\hat{\mathbf{g}}, t) = (\psi(x_1, t), \ldots, \psi(x_n, t))^{\mathsf{T}} \tag{21}$$

are n-collections obtained by evaluating at the observation points a solution of (10) for a given set of parameters $\hat{\mathbf{g}}$.

The cost function is minimized through a Nelder–Mead method which is natively implemented in a Matlab© routine solver [78]. This method is based on an iterative technique to solve nonlinear inverse problems for parameter estimation. By referring to Fig. 5 the routine stops when the residual $\mathscr{R}$ is smaller than a user defined parameter, which in this work is set to 10^{-7}. The default value from the solver is 10^{-4}.

4. Results and Discussions

4.1. Geometry and material parameters

We consider a beam with rectangular cross section. The structural damping parameters are set to $\alpha_w = \alpha_\psi = 10$, see Section 2 for details. The material is characterized by shear modulus ten times smaller than the Young's modulus, and therefore $\alpha_1 = 0.1$. Moreover, we consider the overall shear stiffness $kGA\ell^2$ to be one hundred times larger than the bending stiffness EI, and therefore $\alpha_1\alpha_2 = 100$. Simulations do not require the specification of the scaling time τ; however, the choice of this parameter dictates the density and the length of the device once the shear modulus is given. Simulation scenarios are always set with measuring data set for the vertical and rotational deflection of the system with $\alpha_3 = 10$, meaning that the stiffness of the coupling elements is ten times larger than the shear stiffness of the body so that the body of the sensor morphs according to the shape of the substrate, see [56]. The undisturbed depth of the substrate is set to $d = 1$. The sensor model presented in this work was tested by estimating the viscoelastic parameters of specimens tested in [79], where standard linear viscoelastic material parameters where obtained from experimental data through material response fit.

Fields w and ψ in the reduced order model are both projected on the first two bases functions; this choice is dictated by the necessity to capture even and odd deformation modes (with respect to x) of forcing terms, see Fig. 3.

4.2. Displacement sensor

In this section we present simulation results for the system deployed as a displacement sensor. The implementation of this scenario requires a set of N observation points along the axis of the beam on which strain and/or displacement sensors are installed (typically strain gauges). To induce a deformation of the beam coupled with the substrate we consider two different force inputs. In the first case we consider in (18) $Q_0 = Q_1 = -Q$, while

Table 1
Standard linear viscoelastic material parameters experimentally obtained in [79] for different specimens.

Specimen	β_1	β_2	μ
PH45	0.68	0.39	2.14
PH56	0.56	0.48	5.54
PH76	0.80	0.19	3.76

Table 2
Estimated material properties of a standard linear viscoelastic substrate with step input forces 24.

α_3	α_4	β_1	β_2	β_μ
10	1	0.81	0.19	3.77
10	10	0.79	0.22	3.72
10	20	0.78	0.22	3.71

all the other forcing terms are zero. The forces are applied for 20 nondimensional time units, so that the forcing term becomes

$$\mathbf{F}_w(t) = Q(\bar{\mathbf{w}}(0) + \bar{\mathbf{w}}(1))(\mathfrak{u}(t) - \mathfrak{u}(t-20)) \tag{22}$$

where $\mathfrak{u}$ is the unit step function which evaluates to 1 whenever its argument is greater than 0. In the second case we considered a distributed torque p_c in (18), while the remaining forcing parameters in (18) are zero. The distributed torque is nonzero in the nondimensional time interval $[0, 20]$, so that the expression for p_c is

$$p_c = -T\left(\mathfrak{u}(x) - 2\mathfrak{u}\left(x - \frac{1}{2}\right)\right)(\mathfrak{u}(t) - \mathfrak{u}(t-20)) \tag{23}$$

where T is the nondimensional amplitude of the distributed torque.

Simulated measurements for the cost function (19) were generated by solving (17) for the deformation of the beam when a given set of material parameters are assigned. Simulated measurements are taken with sample rate 1Hz, and unless otherwise specified white noise with standard deviation 4% is added. Material parameters for the beam system are described above, whereas for the substrate we adopted the ones published in [79] and reported in Table 1 in nondimensional form. All numerical examples refer to a system with two observation points at the abscissas $x = 0.5$ and $x = 0.75$ along the axis of the beam. The set of nondimensional beam parameters is completed by considering three cases with $\alpha_4 = (1, 10, 20)$, meaning that the rotational stiffness of the coupling springs could be in the order of the bending stiffness of the body or stiffer. When the displacement is projected on the first two bases functions, the input force (22) with $Q_0 = Q_1 = 1$ is

$$\mathbf{F}_w = \begin{pmatrix} -3.16233 \\ 0 \end{pmatrix}(\mathfrak{u}(t) - \mathfrak{u}(t-20)) \tag{24}$$

Dots and solid lines in Fig. 6 show simulated measurements and displacement solutions for vertical and rotational displacements of the Timoshenko beam from the reduced order model, with $\alpha_3 = 10$ and $\alpha_4 = 10$. The corresponding estimated material properties are shown in the first row of Table 2. These results are in good agreement with the measurements from [79] reported in Table 1 in nondimensional form for comparison. Corresponding deflection $\eta(x)$ of the substrate at $x = 0.5$ is shown in Fig. 7(a) revealing a typical creep response due to a step load history; three snapshots ($t = 16, t = 20$ and $t = 100$) of the deflections of the beam and of the substrate obtained as the solution of the reduced order model are shown in Fig. 7(b), where the horizontal configuration corresponds to unloaded specimen after 80 nondimensional time units the force is released.

For the converged parameters in Table 2, time histories of differences between time-contiguous values $|\beta_i(n+1) - \beta_i(n)|$ $(i = 1, 2, \mu)$ are shown in Fig. 8. Plots show that within few iterations the error drops considerably. Subsequent oscillations are likely due to transients induced in the coupled system. All parameters are fully converged after about 80 iterations. Material parameters reported in Table 2 are considered to be converged when the differences in Fig. 8 are less than or equal the threshold 10^{-4}. For the scenario simulated here, the number of iterations is not a critical parameter as the sensing device does not sense while also locomoting, that is, the device is coupled to the substrate and measurements can continue until deformation transients in the coupled system are dissipated. For applications involving sensing and locomotion, it is crucial to tune system's parameters so that transients in the deformation that affect sensing dissipate much faster than the characteristic rate scale in the locomotion. The formalization of this aspect is the object of current work.

For different values of the coupling elements stiffness $\alpha_4 = (1, 10, 20)$ and for $\alpha_3 = 10$, the converged estimated viscoelastic parameters are summarized in Table 2. Corresponding deflections of the substrate at $x = 0.5$ are shown in Fig. 9(a), and deformed shapes of the beam and of the substrate at $t = 20$ are shown in Fig. 9(b). For the simulated sensor system, increase in α_4 causes an increasing in the beam deflection and consequently in the induced deflection viscoelastic substrate, but material parameters estimation is not significantly affected. On the other hand, increase in α_3 means increasing the stiffness of the coupling springs with respect to the stiffness of the beam, which implies smaller deflections w and η for the same input force. At the limit, for very large α_3, the deflection of the beam would morph on the profile $d(x)$, and therefore very stiff coupling elements would

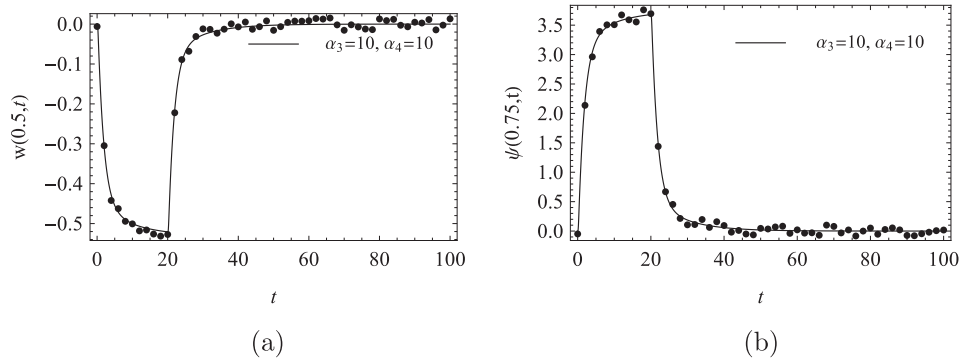

Fig. 6. Simulated measurements (dots) and displacement solutions (solid line) of governing equations of the coupled system (17) for $\alpha_3 = 10$ and $\alpha_4 = 10$ and step input force (24), for (a) vertical displacement, and (b) rotational displacement.

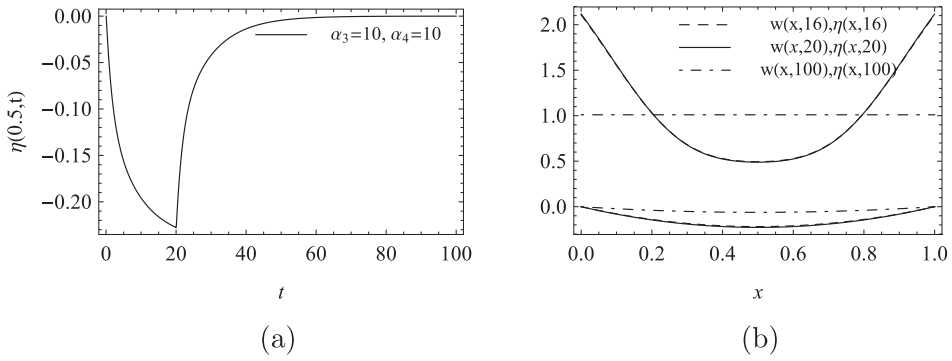

Fig. 7. Plot of (a) time history of the deflection of the substrate at $x = 0.5$; (b) beam and substrate deformed shapes at nondimensional times $t = 16, t = 20, t = 100$, for $\alpha_3 = 10$ and $\alpha_4 = 10$ and step input force (24).

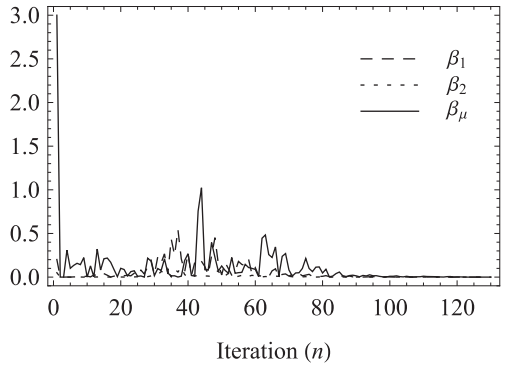

Fig. 8. Time history of the differences $|\beta_i(n+1) - \beta_i(n)|$ $(i = 1, 2, \mu)$ between time-contiguous values of estimated material parameters, versus iteration n.

compromise the functioning of the sensor deployed on an initially flat substrate.

As a second example we consider the input torque (23). For $T = 5$, the projected input torque $\mathbf{F}_\psi$ in (18) is

$$\mathbf{F}_\psi = \begin{pmatrix} 14.04 \\ 0 \end{pmatrix} (\mathrm{u}(t) - \mathrm{u}(t-20)) \tag{25}$$

Table 3 shows the corresponding converged estimated parameters for $\alpha_3 = 10$ and $\alpha_4 = (1, 10, 20)$; also in this case the estimated parameters are in good agreement with the ones reported by [79], and no significant difference is observed with respect to the input considered above. Dots and solid lines in Fig. 10 show simulated measurements and displacement

Table 3
Estimated material properties of a standard linear viscoelastic substrate with step input distributed torque (25).

α_3	α_4	β_1	β_2	β_μ
10	1	0.81	0.19	3.77
10	10	0.81	0.19	3.76
10	20	0.79	0.182	3.76

solutions from the reduced order model, for $\alpha_3 = 10$ and $\alpha_4 = 10$; as before, measurements are simulated with material properties from Table 1, and time history of the displacement is plotted with estimated material parameters from Table 3. Corresponding deflection η of the substrate at $x = 0.5$ is shown in Fig. 11(a), and Fig. 11(b) shows three snapshots ($t = 16, t = 20$ and $t = 100$) of the deflections of the beam and of the substrate obtained as solutions of the reduced order model. Deflection of the substrate at $x = 0.5$ for $\alpha_3 = 10, \alpha_4 = (1, 10, 20)$, and estimated parameters, which are summarized Table 3, are shown in Fig. 12(a), and deflections of the beam and of the substrate for the governing equations of the coupled system for $t = 20$ are shown in Fig. 12(b). Also in this case the displacements are consistent with the expected creep response.

Simulation results were repeated by simulating strain measurements with three different white noise levels and applying the input force in (24), in order to check the robustness of the method with respect to noise. Specifically, measurements were simulated by adding to the model output displacement white noise terms sampled from Gaussian distributions with 2%, 6%, and 10% standard deviations. Noisy displacements for 6% and 10% cases are shown as dots in Fig. 13, along with solid lines showing their

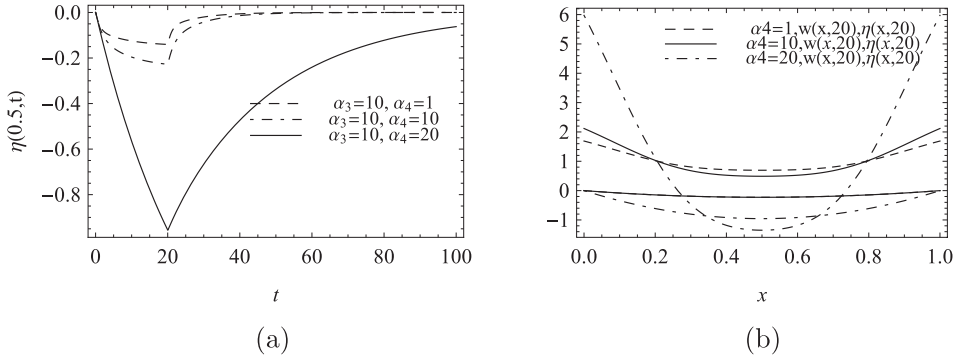

Fig. 9. Plot of (a) Time history of the deflection of the substrate at $x = 0.5$; (b) Beam and substrate deformed shapes at nondimensional times $t = 16, t = 20, t = 100$, for $\alpha_3 = 10$ and $\alpha_4 = (1, 10, 20)$ and step input force (24).

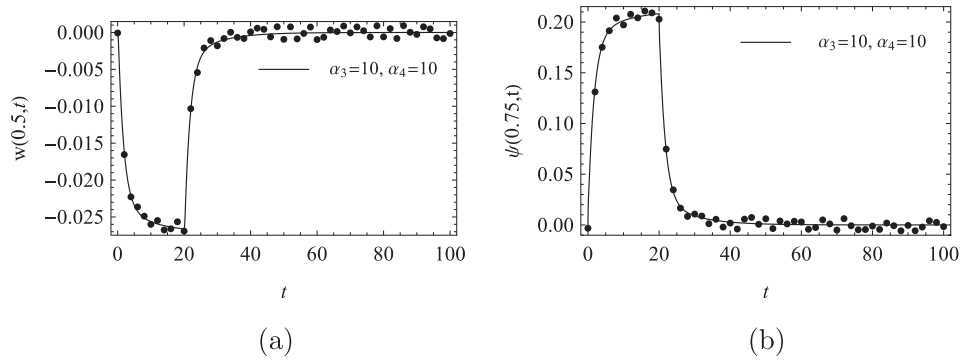

Fig. 10. Simulated measurements (dots) and displacement solutions (solid line) of governing equations of the coupled system (17) for $\alpha_3 = 10$ and $\alpha_4 = 10$ and step torque (25), for (a) vertical displacement, and (b) rotational displacement.

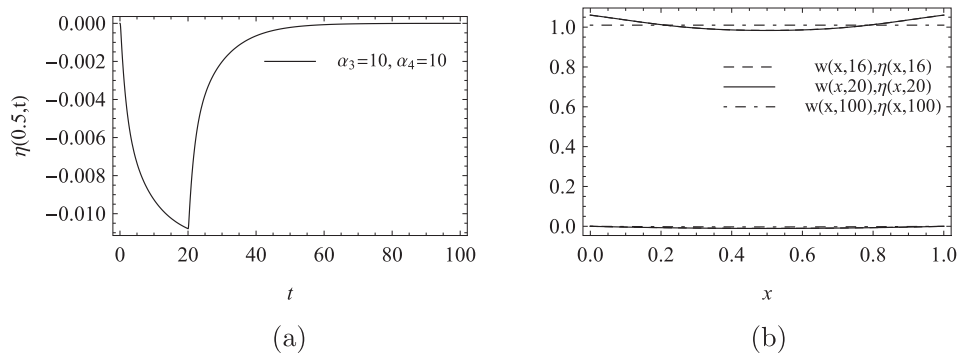

Fig. 11. Plot of (a) time history of the deflection of the substrate at $x = 0.5$; (b) beam and substrate deformed shapes at nondimensional times $t = 16, t = 20, t = 100$, for $\alpha_3 = 10$ and $\alpha_4 = 10$ and step torque (25).

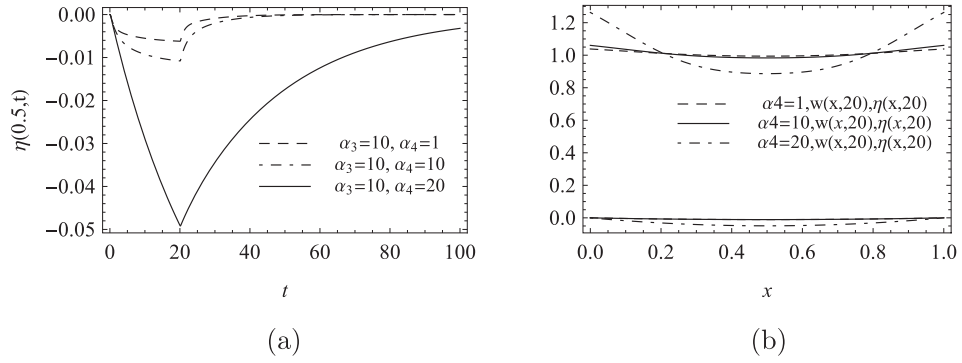

Fig. 12. Plot of (a) time history of the deflection of the substrate at $x = 0.5$; (b) beam and substrate deformed shapes at nondimensional time $t = 20$, for $\alpha_3 = 10$ and $\alpha_4 = (1, 10, 20)$ and step torque (25).

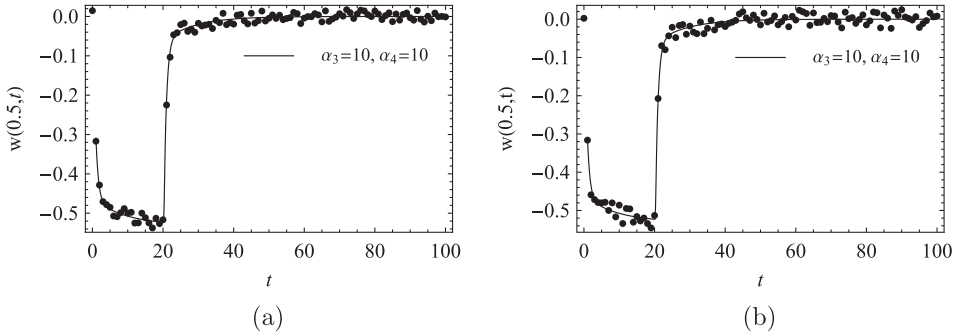

Fig. 13. Simulated measurements (dots) and displacement solutions (solid line) based on estimated parameters in Table 5 with step input force (24) for (a) noisy measurements with standard deviation ±6%, and (b) noisy measurements with standard deviation ±10%.

Table 4
Estimated material properties for the standard linear viscoelastic substrate with respect different noise standard deviations for simulated measurements, $\alpha_3 = 10, \alpha_4 = 10$, and step input force (24).

Noise standard deviation (%)	β_1	β_2	β_μ
2	0.81	0.19	3.76
6	0.81	0.19	3.77
10	0.84	0.21	3.82

Table 5
Estimated material properties for different specimens in [79]. Simulated measurements are obtained for $\alpha_3 = 10, \alpha_4 = 10$, and step input force (24).

Material	β_1	β_2	β_μ
PH45	0.67	0.38	2.13
PH56	0.56	0.47	5.54
PH76	0.81	0.19	3.76

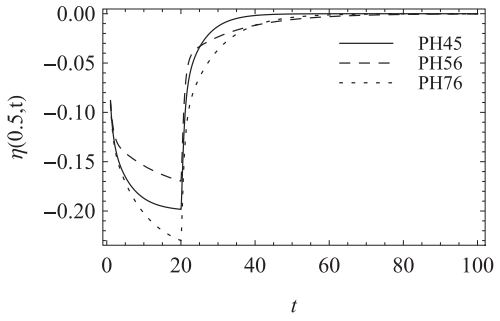

Fig. 14. Simulated substrate displacement at point $x = 0.5$, based on estimated parameters in Table 4 with step input force (24).

common expected values. Estimated material parameters for the three cases are shown in Table 4, revealing a close agreement regardless of the different noises considered. Further increasing of the noise would require the inclusion of noise elimination techniques [80].

In order to check the consistence of the sensor with respect to different specimens, the material property estimation has been repeated by simulating strain measurements with three different specimens presented in Table I of [79] (see Table 1 above). Considering the input force (24) and for $\alpha_3 = 10$ and $\alpha_4 = 10$, Table 5 presents the converged estimated parameters for three specimens, that are in good agreement with the ones experimentally obtained in [79]. Deflections η of these specimens at $x = 0.5$, corresponding to estimated parameters in Table 5, are shown in Fig. 14.

5. Conclusion

We derived the initial boundary values problem governing the evolution of a Timoshenko beam and of the profile of a linear viscoelastic substrate that are coupled through a system of compliant elements. This system has been used as the model to pose an inverse problem for the estimation of the constitutive parameters of the viscoelastic substrate, with material response modeled as standard linear viscoelastic. Material parameters are the minimizing set of a least square cost function encoding the residuals between displacement measurements and model predicted displacements.

Predictions of the sensing apparatus are obtained by simulating the estimation of material parameters for specimens that have been experimentally characterized. Simulated measurements are based on the published values of constitutive viscoelastic parameters. Predictions of the model accurately reproduce published experimental characterizations of standard linear viscoelastic materials, and they show robustness with respect to relatively high white noise added to the simulated measurements.

Current and future work include the hardware realization of the system proposed here, and the experimental testing on soft and biological tissues that typically exhibit viscoelastic responses. The sensor model is being merged with a locomotion and shape morphing model for the same system, with the goal of realizing an autonomous hyper-redundant robotic system that can be deployed in non-structured environments and can be used for sensing, monitoring, and exploring. Device miniaturization allow for sensing of biological tissues with diagnosis related applications.

Conflict of interest

The authors have declared no conflicts of interest.

Acknowledgment

This work was funded by the Natural Sciences and Engineering Research Council of Canada (NSERC) through the Discovery Grant no. 386684/2011.

Appendix A. Basis functions

To obtain the natural frequencies and associated eigenfunctions for w and ψ we follow the approach in [81], which is based on the solution of a vector eigenvalues problem for the system of two coupled second order differential equations for the transverse displacement and for the rotation of the cross section. For the analytical expressions we follow the general procedure that consists on the time-space separation of variables followed by substitution in the homogeneous governing equations. The general solution of the second and third Eqs. (10) with $\alpha_3 = \alpha_4 = 0$ (no forcing terms and no coupling with the substrate) is therefore assumed to be of the form

$$(w(x,t) \quad \psi(x,t))^{\mathsf{T}} = \exp(\mathrm{i}\omega t)(W(x) \quad \Psi(x))^{\mathsf{T}}$$

where ω is the frequency of oscillation, $i = \sqrt{-1}$ is the imaginary unit, and $W(x), \Psi(x)$ are functions in $[0,1]$ that express the dependency on x. By separating the variables and considering the vector evaluated function $\exp(\lambda x)(\overline{W} \quad \bar{\Psi})^{\mathsf{T}}$, where $\overline{W}$ and $\bar{\Psi}$ are constants, in the spatial eigenvalue problem. Spatial eigenvalue function is a solution for some positive constant λ if and only if

$$\begin{pmatrix} \lambda^2 + \beta_1 & -\lambda \\ \beta_3\lambda & \lambda^2 + \beta_2 \end{pmatrix} \begin{pmatrix} \overline{W} \\ \bar{\Psi} \end{pmatrix} = \begin{pmatrix} 0 \\ 0 \end{pmatrix}$$

with nondimensional parameters β_i defined by

$$\beta_1 = \omega^2, \quad \beta_2 = \alpha_1(\omega^2 - \alpha_2), \quad \beta_3 = \alpha_1\alpha_2$$

In order the root of the characteristic polynomial $\lambda^4 + (\beta_1 + \beta_2 + \beta_3)\lambda^2 + \beta_1\beta_2 = 0$ to be real it must be $\Delta > 0$, which is satisfied for $\beta_1\beta_2 < \gamma^2/4$, where $\gamma = \beta_1 + \beta_2 + \beta_3$. The condition $\Delta > 0$ dictates $\omega > 0$; therefore it must be $\gamma > 0$ since this is the case when γ is evaluated for $\omega > 0$. For $\Delta > 0$ and $\gamma > 0$ we have

$$\lambda_1 = \pm i\theta, \quad \theta^2 = \frac{\gamma}{2}\left(\sqrt{\Delta} + 1\right)$$

For $\beta_1\beta_2 < 0$ we have $\sqrt{\Delta} > 1$ and

$$\lambda_2 = \pm\mu, \quad \mu^2 = \frac{\gamma}{2}\left(\sqrt{\Delta} - 1\right)$$

For this case the general solution is therefore given by [81]

$$\Phi(x) = C_1\begin{pmatrix}\sin\theta x\\ -\frac{\beta_1-\theta^2}{\theta}\cos\theta x\end{pmatrix} + C_2\begin{pmatrix}\cos\theta x\\ \frac{\beta_1-\theta^2}{\theta}\sin\theta x\end{pmatrix} + C_3\begin{pmatrix}\sinh\mu x\\ \frac{\beta_1+\mu^2}{\mu}\cosh\mu x\end{pmatrix} + C_4\begin{pmatrix}\cosh\mu x\\ \frac{\beta_1+\mu^2}{\mu}\sinh\mu x\end{pmatrix}$$

Imposing the free end boundary conditions at $x = 0$ we obtain

$$C_1 = C_3\frac{\theta}{\mu} \quad C_2 = -C_4\frac{\beta_1+\mu^2}{\beta_1-\theta^2}$$

By imposing the free end boundary conditions at $x = 1$ we obtain the following linear algebraic relations involving C_3 and C_4

$$\mathbf{A}\begin{pmatrix}C_3\\ C_4\end{pmatrix} = \begin{pmatrix}0\\ 0\end{pmatrix}$$

with coefficients matrix **A** given by

$$\mathbf{A} = \begin{pmatrix}\frac{\theta}{\mu}(\beta_1-\theta^2)\sin\theta + (\beta_1+\mu^2)\sinh\mu & (\beta_1+\mu^2)(\cosh\mu-\cos\theta)\\ -\frac{\beta_1}{\mu}\cosh\mu & -\frac{\beta_1}{\mu}\sinh\mu\end{pmatrix}$$

The nontrivial solutions of the system are obtained by investigating the condition for rank deficiency of the coefficients matrix, which translates to the determinant being zero

$$-\cos\theta\cosh\mu + \frac{\theta(\theta^2-\beta_1)}{\mu(\mu^2+\beta_1)}\sin\theta\sinh\mu + 1 = 0 \tag{A.1}$$

All parameters in the characteristic equation depend on ω and on the material and geometric parameters of the system. Therefore, once the material and the geometry are defined the characteristic equation is a nonlinear function of ω only.

Appendix B. Galerkin projection

The Galerkin projection technique dictates the substitution of (14) into the second and third Eqs. (10) and premultiplication by the sets of test functions $\bar{\mathbf{w}}, \bar{\psi}$, and $\bar{\eta}$ respectively. Integration of the domain of the projected governing equations and integration by parts give

$$\int_0^1 \bar{\mathbf{w}}\left(\bar{\mathbf{w}}^{\mathrm{T}}\ddot{\mathbf{a}} + \frac{\alpha_w}{\omega^\star}\bar{\mathbf{w}}^{\mathrm{T}}\dot{\mathbf{a}} + \alpha_3\bar{\mathbf{w}}^{\mathrm{T}}\mathbf{a}\right)\mathrm{d}x - \int_0^1 \frac{\mathrm{d}\bar{\mathbf{w}}}{\mathrm{d}x}\bar{\psi}^{\mathrm{T}}\mathbf{b}\mathrm{d}x + \int_0^1 \times \frac{\mathrm{d}\bar{\mathbf{w}}}{\mathrm{d}x}\frac{\mathrm{d}\bar{\mathbf{w}}^{\mathrm{T}}}{\mathrm{d}x}\mathbf{a}\mathrm{d}x - \bar{\mathbf{w}}\left(\frac{\mathrm{d}\bar{\mathbf{w}}^{\mathrm{T}}}{\mathrm{d}x}\mathbf{a} - \bar{\psi}^{\mathrm{T}}\mathbf{b}\right)\Big|_0^1 - \int_0^1 \alpha_3\bar{\mathbf{w}}\bar{\eta}\mathrm{d}x = \int_0^1 \bar{\mathbf{w}}p_b\mathrm{d}x \tag{B.1}$$

$$\int_0^1 \bar{\psi}\left(\bar{\psi}^{\mathrm{T}}\ddot{\mathbf{b}} + \frac{\alpha_\psi}{\omega^\star}\bar{\psi}^{\mathrm{T}}\dot{\mathbf{b}} - \alpha_1\alpha_2\left(\frac{\mathrm{d}\bar{\mathbf{w}}^{\mathrm{T}}}{\mathrm{d}x}\mathbf{a} - \bar{\psi}^{\mathrm{T}}\mathbf{b}\right) - \alpha_4\frac{\mathrm{d}\bar{\psi}^{\mathrm{T}}}{\mathrm{d}x}\mathbf{b}\right)\mathrm{d}x + \int_0^1 \frac{\mathrm{d}\bar{\psi}}{\mathrm{d}x}\frac{\mathrm{d}\psi^{\mathrm{T}}}{\mathrm{d}x}\mathbf{b}\mathrm{d}x - \bar{\psi}\frac{\mathrm{d}\bar{\psi}^{\mathrm{T}}}{\mathrm{d}x}\mathbf{b}\Big|_0^1 + \int_0^1 \alpha_4\bar{\psi}\frac{\partial\bar{\eta}}{\partial x}\mathrm{d}x = \int_0^1 \bar{\psi}p_c\mathrm{d}x \tag{B.2}$$

$$\int_0^1 \bar{\eta}\left((\beta_\mu\bar{\eta} + \beta_\mu(\beta_1+\beta_2)\frac{\bar{\eta}}{d})\dot{\mathbf{c}} + (\beta_1\bar{\eta} + \beta_1\beta_2\frac{\bar{\eta}}{d})\mathbf{c}\right)\mathrm{d}x - \int_0^1 \bar{\eta}(\beta_1\bar{\mathbf{w}}\dot{\mathbf{a}} + \beta_2\bar{\mathbf{w}}\mathbf{a})\mathrm{d}x = 0 \tag{B.3}$$

References

[1] A.C. Ramm, Inverse Problems: Mathematical and Analytical Techniques with Applications to Engineering, Springer, USA, 2004.

[2] C. Huang, C. Shih, S. Kim, An inverse vibration problem in estimating the spatial and temporal-dependent external forces for cutting tools, Appl. Math. Model. 33 (6) (2009) 2683–2698.

[3] W. Chen, Y. Yang, W. Chang, H. Lee, Inverse problem of estimating transient heat transfer rate on external wall of forced convection pipe, Energy Convers. Manage. 49 (8) (2008) 2117–2123.

[4] D.T.W. Lin, W. Yan, H. Li, Inverse problem of unsteady conjugated forced convection in parallel plate channels, Int. J. Heat Mass Transfer 51 (5–6) (2008) 993–1002.

[5] M. Girault, D. Petit, Resolution of linear inverse forced convection problems using model reduction by the modal identification method: application to turbulent flow in parallel-plate duct, Int. J. Heat Mass Transfer 47 (17–18) (2004) 3909–3925.

[6] C. Huang, W. Chen, A three-dimensional inverse forced convection problem in estimating surface heat flux by conjugate gradient method, Int. J. Heat Mass Transfer 43 (17) (2000) 3171–3181.

[7] B. Barabasz, E. Gajda-Zagorska, S. Migorski, M. Paszynski, R. Schaefer, M. Smolka, A hybrid algorithm for solving inverse problems in elasticity, Int. J. Appl. Math. Comput. Sci. 24 (4) (2014) 865–886, http://dx.doi.org/10.2478/amcs-2014-0064.

[8] T. Faurholdt, Inverse modelling of constitutive parameters for elastoplastic problems, J. Strain Anal. Eng. Des. 35 (6) (2000) 471–478, http://dx.doi.org/10.1243/0309324001514233.

[9] G. Lubineau, A. Moussawi, J. Xu, R. Gras, A domain decomposition approach for full-field measurements based identification of local elastic parameters, Int. J. Solids Struct. 55 (SI) (2015) 44–57, http://dx.doi.org/10.1016/j.ijsolstr.2014.11.009.

[10] G. Bal, C. Bellis, S. Imperiale, F. Monard, Reconstruction of constitutive parameters in isotropic linear elasticity from noisy full-field measurements, Inverse Problems 30 (12). http://dx.doi.org/10.1088/0266-5611/30/12/125004.

[11] G. Zhang, H. Yang, Y. Xu, A surrogate-model-based identification of fractional viscoelastic constitutive parameters, Mech. Time-Dependent Mater. 19 (1) (2015) 1–19, http://dx.doi.org/10.1007/s11043-014-9245-5.

[12] M. Tartibi, D.J. Steigmann, K. Komvopoulos, A reverse updated Lagrangian finite element formulation for determining material properties from measured force and displacement data, Comput. Mech. 54 (6) (2014) 1375–1394, http://dx.doi.org/10.1007/s00466-014-1064-7.

[13] T. Knabe, H.F. Schweiger, T. Schanz, Calibration of constitutive parameters by inverse analysis for a geotechnical boundary problem, Canadian Geotech. J. 49 (2) (2012) 170–183, http://dx.doi.org/10.1139/T11-091.

[14] W. Chen, Dynamic modeling of multi-link flexible robotic manipulators, J. Comput. Struct. 79 (2001) 183–195.

[15] B.-J. Lee, Geometrical derivation of differential kinematics to calibrate model parameters of flexible manipulator, Int J Adv Robot Syst 10 (2013) 106, http://dx.doi.org/10.5772/55592.

[16] L. Chen, H. Deng, Model reduction of rigid-flexible manipulators with experimental validation, in: 3rd International Conference on Advances in Materials Manufacturing (ICAMMP 2012), vol. 655–657, Beihai, PR China, Dec 22–23, 2012, pp. 1101–1107.

[17] H. Esfandiar, S. Daneshmand, Complete dynamic modeling and approximate state space equations of the flexible link manipulator, J. Mech. Sci. Technol. 26 (9) (2012) 2845–2856.

[18] C. di Castri, A. Messina, Exact modeling for control of flexible manipulators, J. Vibr. Control 18 (10) (2012) 1526–1551.

[19] M.H. Korayem, H.N. Rahimi, A. Nikoobin, Mathematical modeling and trajectory planning of mobile manipulators with flexible links and joints, Appl. Math. Model. 36 (7) (2012) 3223–3238, http://dx.doi.org/10.1016/j.apm.2011.10.002.

[20] H. Lee, C. Richards, R. Richards, Experimental and numerical study of microchannel heater/evaporators for thermal phase-change actuators, Sens. Actuat. A: Phys. 195 (2013) 7–20.

[21] H.V. Thakur, S.M. Nalawade, Y. Saxena, K. Grattan, All-fiber embedded pm-pcf vibration sensor for structural health monitoring of composite, Sens. Actuat. A: Phys. 167 (2) (2011) 204–212.

[22] W.Q., W.Y., Z.L., Inverse mode problem in the discrete model of circular plate axial symmetry vibration, in: International Conference on Mechanical Engineering and Green Manufacturing (MEGM), 2010, pp. 71–78.

[23] B.N. Datta, V. Sokolov, Quadratic inverse eigenvalue problems, active vibration control and model updating, Appl. Comput. Math. 8 (2) (2009) 170–191.

[24] L.D. Chiwiacowsky, H.F. De Campos Velho, P. Gasbarri, A variational approach for solving an inverse vibration problem, Inverse Problems in Science and Engineering 14 (5) (2006) 557–577, Symposium on Inverse Problems, Design and Optimization, Rio de Janeiro, Brazil, Mar 17–19, 2004. http://dx.doi.org/10.1080/17415970600574237.

[25] C. Liu, An iterative GL(n,R) method for solving non-linear inverse vibration problems, Nonlinear Dyn. 74 (3) (2013) 685–699, http://dx.doi.org/10.1007/s11071-013-0997-2.

[26] A. Maciag, A. Pawinska, Solving direct and inverse problems of plate vibration by using the Trefftz functions, J. Theor. Appl. Mech. 51 (3) (2013) 543–552.

[27] G.F. Safina, Analysis of direct and inverse problems on transverse vibrations of a supported shaft, Russ. J. Nondestruct. Testing 46 (4) (2010) 302–313, http://dx.doi.org/10.1134/S106183091004008X.

[28] K.M. Dolatshahi, F.R. Rofooei, Inverse vibration problem for un-damped 3-dimensional multi-story shear building models, J. Sound Vibr. 333 (1) (2014) 99–113, http://dx.doi.org/10.1016/j.jsv.2013.08.045.

[29] H. Ressing, M. Gadala, A practical investigation to solving the inverse problem of crack identification through vibration measurements, Eng. Comput. 23 (1–2) (2006) 32–56, http://dx.doi.org/10.1108/02644400610638961.
[30] N. Khiem, Crack detection for structure based on the dynamic stiffness model and the inverse problem of vibration, Inverse Problems Sci. Eng. 14 (1) (2006) 85–96, http://dx.doi.org/10.1080/17415970500272908.
[31] C. Huang, A generalized inverse force vibration problem for simultaneously estimating the time-dependent external forces, Appl. Math. Model. 29 (11) (2005) 1022–1039, http://dx.doi.org/10.1016/j.apm.2005.02.006.
[32] C. Huang, A nonlinear inverse problem in estimating simultaneously the external forces for a vibration system with displacement-dependent parameters, J. Franklin Inst. Eng. Appl. Math. 342 (7) (2005) 793–813, http://dx.doi.org/10.1016/j.jfranklin.2005.06.006.
[33] C. Huang, A non-linear inverse vibration problem of estimating the external forces for a system with displacement-dependent parameters, J. Sound Vibr. 248 (5) (2001) 789–807, http://dx.doi.org/10.1006/jsvi.2001.3838.
[34] G. Gladwell, Inverse Problems in Vibration (Mechanics: Dynamical Systems), 9, Martinus Nijhoff Publishers, 1986.
[35] D. Moss, H. Benaroya, A discrete inverse vibration problem with parameter uncertainty, Appl. Math. Comput. 69 (2–3) (1995) 313–333, http://dx.doi.org/10.1016/0096-3003(94)00140-Y.
[36] L. Starek, D. Iman, A. Kress, A symmetric inverse vibration problem, J. Vibr. Acoust. 114 (4) (1992) 564–568, http://dx.doi.org/10.1115/1.2930299.
[37] M. Yamamoto, Inverse eigenvalue problem for a vibration of a string with viscous drag, J. Math. Anal. Appl. 152 (1) (1990) 20–34, http://dx.doi.org/10.1016/0022-247X(90)90090-3.
[38] H. Banks, R. Powers, I. Rosen, Inverse problems in the modeling of vibrations of flexible beams, Lect. Notes Control Inf. Sci. 102 (1987) 1–22.
[39] A. Tsaune, V. Golovko, Anharmonic vibration–rotation inverse problem with reconstruction of Hamiltonian terms, J. Mol. Spectrosc. 108 (1) (1984) 82–98, http://dx.doi.org/10.1016/0022-2852(84)90288-1.
[40] M. Hamada, Y. Seguchi, Y. Tada, Shape determination problems of structures by the inverse variational principle: 2nd report, buckling and vibration problems, Jpn. Soc. Mech. Eng. Bull. JSME 23 (184) (1980) 1581–1588.
[41] N. Stepanov, G. Koptev, Y. Panchenko, Uniqueness of solution of an inverse vibration problem, Optika i spektroskopiya 38 (4) (1975) 657–662.
[42] J. Humphrey, Continuum biomechanics of soft biological tissues, Proc. Roy. Soc. A: Math. Phys. Eng. Sci. 459 (2029) (2003) 3–46, http://dx.doi.org/10.1098/rspa.2002.1060.
[43] Y. Fung, Biomechanics-Mechanical Properties of Living Tissues, Springer, 1993.
[44] M.D. Maestro, F. Cecchi, S.M. Serio, C. Laschi, P. Dario, Sensing device for measuring infants grasping actions, Sens. Actuat. A – Phys. 165 (2011) 155–163, http://dx.doi.org/10.1016/j.sna.2010.08.016.
[45] M. Morris, F. Huxham, J. McGinley, K. Dodd, R. Iansek, The biomechanics and motor control of gait in Parkinson disease, Clin. Biomech. 16 (6) (2001) 459–470, http://dx.doi.org/10.1016/S0268-0033(01)00035-3.
[46] G.Y.H. Lee, C.T. Lim, Biomechanics approaches to studying human diseases, Trends Biotechnol. 25 (3) (2007) 111–118, http://dx.doi.org/10.1016/j.tibtech.2007.01.005.
[47] E.J. Weinberg, D. Shahmirzadi, M. Mofrad, On the multiscale modeling of heart valve biomechanics in health and disease, Biomech. Model. Mechanobiol. 9 (4) (2010) 373–387, http://dx.doi.org/10.1007/s10237-009-0181-2.
[48] M.K. Rausch, E. Kuhl, On the effect of prestrain and residual stress in thin biological membranes, J. Mech. Phys. Solids 61 (9) (2013) 1955–1969, http://dx.doi.org/10.1016/j.jmps.2013.04.005.
[49] L.M. Sander, Alignment localization in nonlinear biological media, Biomech. Eng. 135 (7) (2013) 71006, http://dx.doi.org/10.1115/1.4024199.
[50] A.M. Zoellner, A.B. Tepole, E. Kuhl, On the biomechanics and mechanobiology of growing skin, J. Theor. Biol. 297 (2012) 166–175, http://dx.doi.org/10.1016/j.jtbi.2011.12.022.
[51] W. Liu, D. Li, J. Shen, Least-squares solutions of constrained inverse eigenproblem and associated optimal approximation problem, Int. J. Comput. Math. 90 (3) (2013) 641–650, http://dx.doi.org/10.1080/00207160.2012.735662.
[52] M.S. Gockenbach, A.A. Khan, An abstract framework for elliptic inverse problems: part 1, an output least-squares approach, Math. Mech. Solids 12 (3) (2007) 259–276, http://dx.doi.org/10.1177/1081286505055758.
[53] R. Forke, D. Scheibner, K. Hiller, T. Gessner, W. Dötzel, J. Mehner, Fabrication and characterization of a force coupled sensor–actuator system for adjustable resonant low frequency vibration detection, Sens. Actuat. A: Phys. 145 (2008) 245–256.
[54] C. Yang, Solution of an inverse vibration problem using a linear least-squares error method, Appl. Math. Model. 20 (10) (1996) 785–788.
[55] D. Hua, P. Lancaster, Linear matrix equations from an inverse problem of vibration theory, Linear Algebra Appl. 246 (1996) 31–47.
[56] J. Fattahi, D. Spinello, A Timoshenko beam reduced order model for shape tracking with a slender mechanism, J. Sound Vibr. 333 (20) (2014) 5165–5180, http://dx.doi.org/10.1016/j.jsv.2014.05.040.
[57] J. Fattahi, D. Spinello, Timoshenko beam model for exploration and sensing with a continuum centipede inspired robot, in: Proceedings of 2013 ASME Dynamic Systems and Control Conference, vol. 5391, 2013, pp. 189–196. doi:http://dx.doi.org/10.1117/12.546606.
[58] R.W. Cahn, Biomimetics: biologically inspired technologies, Nature 444 (7118) (2006) 425–426, http://dx.doi.org/10.1038/444425b.
[59] L. Drago, G. Fusco, E. Garollo, A. Minelli, Structural aspects of leg-to-gonopod metamorphosis in male helminthomorph millipedes (Diplopoda), Front. Zoology 8. http://dx.doi.org/10.1186/1742-9994-8-19.
[60] M. Golubitsky, I. Stewart, P. Buono, J. Collins, A modular network for legged locomotion, Phys. D 115 (1–2) (1998) 56–72, http://dx.doi.org/10.1016/S0167-2789(97)00222-4.
[61] L.D. Landau, E.M. Lifshitz, Theory of Elasticity, Vol. 7 of a Course of Theoretical Physics, Pergamon Press, 1970.
[62] S. Timoshenko, Vibration Problems in Engineering, D. Van Nostrand Company Inc., 1974.
[63] L. Meirovitch, Fundamentals of Vibrations, McGraw-Hill, 2001.
[64] A. Plaseied, A. Fatemi, Deformation response and constitutive modeling of vinyl ester polymer including strain rate and temperature effects, J. Mater. Sci. 43 (4) (2008) 1191–1199, http://dx.doi.org/10.1007/s10853-007-2297-z.
[65] A.D. Kerr, Elastic and viscoelastic foundation models, J. Appl. Mech. 31 (1964) 491, http://dx.doi.org/10.1115/1.3629667.
[66] S.C. Dutta, R. Roy, A critical review on idealization and modeling for interaction among soil-foundation-structure system, Comput. Struct. 80 (20–21) (2002) 1579–1594, http://dx.doi.org/10.1016/S0045-7949(02)00115-3.
[67] D.N. Paliwal, S.N. Sinha, Static and dynamic behavior of shallow spherical-shells on Winkler foundation, Thin-Walled Struct. 4 (6) (1986) 411–422, http://dx.doi.org/10.1016/0263-8231(86)90038-8.
[68] M.M. Filonenko-Borodich, Some approximate theories of the elastic foundation, Uchenyie Zapiski Moskovskogo Gosudarstuennogo Universiteta, Mechanika 46 (1940) 1–3 (in Russian).
[69] P.L. Pasternak, On a New Method of Analysis of an Elastic Foundation by Means of Two Foundation Constants, Gosudarsrvennoe Izdatelstvo Literaturi po Stroitelstvu i Arkhitekture (in Russian).
[70] I. Calio, A. Greco, Free vibrations of Timoshenko beam-columns on Pasternak foundations, J. Vibr. Control 19 (5) (2013) 686–696, http://dx.doi.org/10.1177/1077546311433609.
[71] C.R. Briscoe, S.C. Mantell, J.H. Davidson, Buckling of a plate on a Pasternak foundation under uniform in-plane bending loads, Int. J. Struct. Stability Dyn. 13 (3) (2013) 1250070, http://dx.doi.org/10.1142/S0219455412500708.
[72] R. Jones, J. Xenophontos, The Vlasov foundation model, Int. J. Mech. Sci. 19 (6) (1977) 317–323.
[73] V.Z. Vlasov, U. Leont'ev, Beams, Plates, and Shells on Elastic Foundation, Gosudarst vennoe Izdatel'st vo Ftziko-Matematicheskoi Literatury Moskva.
[74] M. Levinson, Generalized Vlasov-Jones foundation model – a foundation of grade-4, Int. J. Mech. Sci. 25 (2) (1983) 149–154, http://dx.doi.org/10.1016/0020-7403(83)90007-3.
[75] A. Shams, M. Porfiri, A generalized Vlasov-Jones foundation model for micromechanics studies of syntactic foams, Compos. Struct. 103 (2013) 168–178, http://dx.doi.org/10.1016/j.compstruct.2013.04.020.
[76] F. Zhaohua, D.R. Cook, Beam elements on two-parameter elastic foundation, J. Eng. Mech. 109 (6) (1983) 1390–1402.
[77] M. Kneifati, Analysis of plates on a Kerr foundation model, J. Eng. Mech. 111 (11) (1985) 1325–1342, http://dx.doi.org/10.1061/(ASCE)0733-9399(1985)111:11(1325).
[78] M. Works, fminsearch, <http://www.mathworks.com/help/matlab/ref/fminsearch.html> (Release 12).
[79] D. Craiem, F.J. Rojo Pérez, J.M. Atienza Riera, G.V. Guinea Tortuero, R.L. Armentano, Fractional calculus applied to model arterial viscoelasticity, Latin Am. Appl. Res. 38 (2) (2008) 141–145.
[80] R. Myers, Classical and Modern Regression with Applications, Duxbury Classic Series, Duxbury/Thompson Learning, 1990.
[81] N.F.J. van Rensburg, A.J. van der Merwe, Natural frequencies and modes of a Timoshenko beam, Wave Motion 44 (1) (2006) 58–69, http://dx.doi.org/10.1016/j.wavemoti.2006.06.008.